An energy balance perspective on regional CO_2-induced temperature changes in CMIP5 models

Jouni Räisänen

Department of Physics, University of Helsinki

Submitted to Climate Dynamics, 8 March 2016

Revised, 6 June 2016

Corresponding author

Jouni Räisänen

Department of Physics, P.O. Box 48, FI-00014 University of Helsinki, Finland

Phone +358-2941 50872

Email: jouni.raisanen@helsinki.fi

Abstract

An energy balance decomposition of temperature changes is conducted for idealized transient CO_2-only simulations in the fifth phase of the Coupled Model Intercomparison Project (CMIP5). The multimodel global mean warming is dominated by enhanced clear-sky greenhouse effect due to increased CO_2 and water vapour, but other components of the energy balance substantially modify the geographical and seasonal patterns of the change. Changes in the net surface energy flux are important over the oceans, being especially crucial for the muted warming over the northern North Atlantic and for the seasonal cycle of warming over the Arctic Ocean. Changes in atmospheric energy flux convergence tend to smooth the gradients of temperature change and reduce its land-sea contrast, but they also amplify the seasonal cycle of warming in northern North America and Eurasia. The three most important terms for intermodel differences in warming are the changes in the clear-sky greenhouse effect, clouds, and the net surface energy flux, making the largest contribution to the standard deviation of annual mean temperature change in 34%, 29% and 20% of the world, respectively. Changes in atmospheric energy flux convergence mostly damp intermodel variations of temperature change especially over the oceans. However, the opposite is true for example in Greenland and Antarctica, where the warming appears to be substantially controlled by heat transport from the surrounding sea areas.

KEYWORDS: temperature change, energy budget, atmospheric heat convergence, surface energy flux, CMIP5

1. Introduction

Increases in CO_2 and other greenhouse gases make the atmosphere less transparent in the thermal infrared area, thus reducing the outgoing longwave radiation (OLR). The resulting surplus of energy warms the surface and the lower atmosphere. This warming increases OLR, thereby reducing the energy imbalance (e.g. Houghton 2015). However, the outcome of this process in terms of the resulting near-surface temperature change is affected by several feedbacks that alter the fluxes of energy in the climate system.

The equilibrium global and annual mean temperature response to increasing CO_2 is commonly analysed in terms of the water vapour, lapse rate, cloud and surface albedo feedbacks (Hansen et al. 1984; Flato et al. 2013). Typically the results are expressed in terms of feedback factors that relate the change in the top-of-the-atmosphere (TOA) radiation balance to the near-surface temperature change. However, it is also possible to diagnose the contributions of the direct CO_2 forcing and the feedbacks to the temperature change (Dufresne and Bony 2008; hereafter DB08), although the nonlinearity of the problem makes this decomposition mathematically non-unique (Caldwell et al. 2016). In energy balance analysis of transient climate change, ocean heat uptake must be included in addition to the processes that regulate the equilibrium warming (Gregory and Mitchell 1997; DB08).

When considering temperature change at regional scales, the effects of atmospheric energy transport also need to be implicitly or explicitly included (e.g. Boer and Yu 2003). Recently, two techniques have been proposed for diagnosing the energetic contributors to regional temperature change: the surface energy budget approach of Izumi et al. (2015; herafter IBH15) and the climate feedback-response analysis method (CFRAM) introduced by Lu and Cai (2009).

IBH15 applied their method to ensemble mean temperature changes from six models in the fifth phase of the Coupled Model Intercomparison Project (CMIP5). The warming in simulations with quadrupled CO_2 was found to be strongly dominated by increased clear-sky downward longwave (LW) radiation, which was partly compensated by a widespread increase in latent heat flux and reduced clear-sky downward shortwave (SW) radiation mainly caused by increased water vapor absorption in the atmosphere. Similar findings with signs reversed applied to simulations for the Last Glacial Maximum, but the change in surface albedo contributed much more to the glacial cooling than to the CO_2-induced warming. In both cases, variations in the clear-sky downward LW radiation dominated the geographical variations of temperature change, although several other terms also contributed.

In CFRAM, the temperature changes associated with each individual process are solved in the atmosphere-surface column, using a one-dimensional energy balance equation that incorporates the local and non-local effects of temperature change on the LW radiation transfer. Taylor et al. (2013) used this method to show that the polar amplification of the simulated CO_2-induced warming in the NCAR CCSM4 model was mostly due to the surface albedo feedback. Sejas et al. (2014a) used the same method to analyse the seasonal cycle of temperature changes in the same model. In particular, they demonstrated the importance of ocean heat storage changes in shifting the maximum of polar warming from summer (when the albedo feedback is greatest) to late autumn and winter.

CFRAM and the IBH15 surface energy balance approach both have their strengths and limitations. CFRAM is more detailed in terms of the processes considered, but requires a relatively sophisticated calculation of radiative transfer which makes it more challenging to apply to a large ensemble of model simulations. The IBH15 method is more straightforward and only requires a limited number of two-dimensional model fields. On the other hand, as this approach is entirely based on the surface energy budget, the results are disconnected from studies that use the TOA radiation balance for analysis of global mean temperature change. The strong dominance of the clear-sky downward LW radiation in explaining the magnitude and patterns of surface temperature change may also be regarded as a complicating feature. Separation between cause and effect is difficult in this case, because much of the downward LW radiation originates from the lowest atmospheric layers whose temperature is closely correlated with the surface temperature (Zhao et al. 1994).

Here, we propose an alternative method for studying the energy balance contributions to regional temperature change. The method was introduced in Räisänen and Ylhäisi (2015; hereafter RY15) but is here refined for its treatment of SW radiation. Only two-dimensional surface and TOA model output is needed, which makes the method convenient to apply to large ensembles of model simulations. On the other hand, the diagnostics obtained from this method are easier to compare with the traditional global TOA radiation balance approach than is the case with a surface energy budget method.

We apply our method to idealized transient CO_2 experiments from 16 CMIP5 models, analysing both the multimodel mean changes and the contributions of different energy balance processes to the intermodel differences in temperature change. A general finding from our research is that the energetics of temperature change are highly regionally variable. For example, while cloud feedbacks have been identified as the main uncertainty in the global mean temperature change (Flato et al. 2013, Vial et al. 2013), their contribution is not dominant in all seasons and all areas.

The model output used for the study is detailed in Section 2. The energy balance framework is described in Section 3. The results are covered in Section 4, starting from global and regional annual mean temperature changes and then proceeding to the seasonality of the changes in selected regions. In the end of the section, the role of atmospheric energy transport changes in modulating the temperature changes is discussed in some more depth. The main conclusions are presented in Section 5.

2. Data sets and data processing

Monthly data for 16 CMIP5 models were used: ACCESS1-3, BCC-CSM1-1, BCC-CSM1-1-m, CanESM2, CESM1-BGC, GFDL-CM3, INM-CM4, IPSL-CM5A-MR, IPSL-CM5B-LR, MIROC5, MIROC-ESM, MPI-ESM-LR, MPI-ESM-MR, MRI-CGCM3, NorESM1-M and NorESM1-ME, where the acronyms follow Table 9.1 in Flato et al. (2013). This includes all the models for which the required variables could be retrieved both for the preindustrial control simulation (*piControl*) and the simulation with CO_2 increasing 1 % per year compound (*1pctCO₂*) until the quadrupling of CO_2 in 140 years. Only one realization of these two simulations (*r1i1p1*) was used for each model. All the model data were interpolated to a common 2.5 × 2.5 degrees latitude-longitude grid using the Climate Data Operators (https://code.zmaw.de/projects/cdo) first-order conservative remapping (*remapcon*).

The 15 variables used are listed in Table 1. In the energy balance analysis described in Section 3, their decadal monthly means from the *1pctCO2* and *piControl* simulations were first used to calculate the temperature change and its various components for each decade and month. Then the changes were averaged over the six decades centred at the doubling of CO_2 (years 41-100). Conventionally, the transient climate response is defined using bidecadal means over the years 61-80 (Cubasch et al. 2001). A longer averaging period is preferred here because it helps to reduce internal variability, which would have a large effect on the monthly mean changes in the individual models if bidecadal means were used. However, the multimodel mean results are only modestly affected by this difference in periods. The multimodel global mean warming is 1.78 K for the years 61-80 and 1.82 K for the years 41-100.

When calculating statistics for land and sea areas separately, a common land sea mask (from the National Centers for Environmental Prediction – National Center for Atmospheric Research reanalysis) is used. This choice is preferred for simplicity, even though it may induce some “leakage” between land and sea in the individual models.

.

3. Energy balance framework

To relate the changes in surface air temperature with the atmospheric energy budget, a modified version of the method of RY15 was used. As discussed below, this method is rough in its treatment of LW radiation. However, the adoption of the approximate partial radiative perturbation (APRP) method (Taylor et al. 2007) allows a cleaner separation of shortwave (SW) radiative feedbacks than in RY15.

The rate of change of total energy in an atmospheric column is

$$\frac{\partial E}{\partial t} = S - L - G + C \qquad (1)$$

where S is net SW radiation at the TOA, L outgoing LW radiation at the TOA, G net downward heat flux to the surface and C horizontal energy flux convergence in the atmosphere. To relate (1) with the surface air temperature T, we write

$$L = \varepsilon_{eff}\,\sigma T^4 \qquad (2)$$

where ε_{eff} is an effective planetary emissivity. ε_{eff} is essentially a measure of the atmospheric greenhouse effect, although it is also to some extent affected by variations in the surface emissivity, the surface-to-air temperature difference, and short-term (below decadal monthly means) temperature variations. However, an inspection of the surface upwelling LW radiation in the CMIP5 models confirmed that these latter factors are generally unimportant for the changes in ε_{eff}. Substituting (2) into (1), one obtains

$$\varepsilon_{eff}\,\sigma T^4 = S - G + (C - \frac{\partial E}{\partial t}) \qquad (3)$$

Letting now $\Delta X = X_2 - X_1$ denote the change in quantity X between two climates (1 = baseline CO_2, 2 = increased CO_2) and $[X]$ the mean of these two, (3) gives

$$\sigma\left[\varepsilon_{eff}\right]\Delta(T^4) = \underbrace{-\sigma\Delta\varepsilon_{eff}\left[T^4\right]}_{I} + \underset{II}{\Delta S}\ \underset{III}{-\Delta G} + \underbrace{\Delta(C - \frac{\partial E}{\partial t})}_{IV} \qquad (4)$$

Finally, linearizing the left side of (4) as

$$\sigma[\varepsilon_{eff}]\Delta(T^4) \approx 4\sigma[\varepsilon_{eff}][T]^3\Delta T = D\Delta T \qquad (5)$$

allows one to decompose the simulated temperature change as

$$\Delta T = \underset{I}{LW} + \underset{II}{SW} + \underbrace{SURF}_{III} + \underbrace{CONV}_{IV} + ERR \qquad (6)$$

where the terms *I–IV* in (4) have been divided by $D = 4\sigma[\varepsilon_{eff}][T]^3$. *LW* represents the temperature change caused by the change in ε_{eff} and *SW* that due to the change in the net TOA SW radiation. *SURF* is negative when the net downward heat flux at the surface increases. *CONV* is evaluated as a residual of the energy budget. RY15 denoted this term as *CONV* – *STOR* to emphasize that the changes in both the atmospheric horizontal energy flux convergence and local atmospheric storage are included. However, at least for annual means it is safe to assume that the change in energy flux convergence dominates (RY15). *ERR* results from the linearization in (5) but turns out to be very small (Section 4.1).

ε_{eff} in (2) is affected by atmospheric LW opacity and the vertical lapse rate of temperature, but is largely insensitive to vertically uniform temperature changes. Consequently, the coefficient *D* in (5) is a good approximation of the Planck feedback parameter. It has a multimodel global and annual mean value of 3.3 $Wm^{-2} K^{-1}$, whereas the Planck feedback parameter is close to 3.2 $Wm^{-2} K^{-1}$ in both the CMIP3 and CMIP5 models (Soden and Held 2006; Flato et al. 2013). Thus, in the conversion from (4) to (6), an energy flux perturbation of 1 Wm^{-2} is typically equivalent to a 0.3 K change in temperature, although the precise value varies with month, model and geographic location.

By using the TOA all-sky (*rlut*) and clear-sky (*rlutcs*) LW fluxes, *LW* is further divided into clear-sky and cloud radiative effect contributions.

$$LW = LW_{CLEAR} + LW_{CRE} \tag{7}$$

In broad terms, LW_{CLEAR} incorporates the LW radiative forcing due to increasing CO_2 together with the water vapour and the lapse rate feedbacks, whereas LW_{CRE} represents the change in the LW cloud radiative effect (CRE). Unfortunately, LW_{CRE} is a negatively biased approximation of the actual LW cloud feedback, because increases in CO_2 and water vapor act to reduce the effect of clouds on the OLR (Section 4.1).

The treatment of SW radiation is based on the APRP method. Using the TOA and surface all-sky and clear-sky SW fluxes and total cloudiness, the change in the TOA net SW radiation is divided to five components, which are further converted to the corresponding temperature changes as

$$SW = SW_{IN} + SW_{CLEAR-ATM} + SW_{ALBEDO} + SW_{CLOUD} + SW_{NL} \tag{8}$$

The first term in (8) accounts for the change in the TOA incoming solar radiation (ΔS in Eq. (6) of Taylor et al. 2007), whereas the next three terms represent the changes in the SW radiative properties of the clear-sky atmosphere, surface albedo, and clouds (Eqs. (16a-c) of Taylor et al. 2007). Higher-order nonlinear effects are collected in the last term. Note that SW_{CLOUD} represents, within the accuracy of the APRP method, the actual SW cloud feedback rather than the change in SW CRE. In particular, this avoids the aliasing of surface albedo and cloud change contributions in the SW radiation budget that affects the changes in SW CRE (Qu and Hall 2006; RY15).

4. Results

4.1 Global and local mean values

The magnitude of the various terms in (6)-(8) is explored in Table 2. The first three columns give their multimodel annual means for the globe and land and sea areas separately. For the remaining columns, the absolute values of the terms are averaged over all individual models, months and grid boxes, so to avoid compensation between positive and negative values. We first note that SW_{IN}, SW_{NL} and ERR are negligible, with values of $\leq 10^{-3}$ K in all cases. ERR is much smaller than the linearization residuals in Taylor et al. (2013), Sejas et al. (2014a,b) and IBH15. This is achieved by conducting the linearization in (5) around the average of the baseline and perturbed temperatures rather than the baseline mean.

The multimodel global annual mean warming of 1.82 K is dominated and actually exceeded by LW_{CLEAR} (2.07 K). Other terms that enhance the warming include $SW_{CLEAR\text{-}ATM}$ (0.21 K), SW_{ALBEDO} (0.19 K) and SW_{CLOUD} (0.13 K). The first of these reflects stronger absorption of solar near-infrared radiation by increased CO_2 and water vapour, the second the effects of reduced snow and ice cover, and the third reduced cloud cover over many low-to-mid-latitude areas. The warming is counteracted by $SURF$ (-0.39 K), due to ocean heat uptake during transient CO_2 increase, and LW_{CRE} (-0.39 K).

The global means for $SURF$ and SW_{ALBEDO} are very close to those reported by DB08 for their sample of 12 CMIP3 models (transient temperature changes for “Albedo” and “OHU efficiency” in their Table 3). This results from the close similarity between D in (5) and the Planck feedback parameter used to convert the energy flux perturbations to temperature changes in DB08. However, the sum of SW_{CLOUD} and LW_{CRE} (hereafter *CLOUD*) gives a net cloud contribution of -0.26 K, in stark contrast with the mean cloud feedback of 0.4 K found by DB08. Studies with CMIP5 models also support a predominantly positive net cloud feedback and, in particular, a positive LW cloud feedback in nearly all models (Tomassini et al. 2013; Vial et al. 2013; see also Fig. 7.10 of Boucher et al. 2013 and Table 9.5 of Flato et al. 2013). This discrepancy arises because LW_{CRE} is calculated directly from the change in the LW CRE, instead of a radiative kernel or a partial radiative perturbation approach that would explicitly isolate the effect of cloud changes (Soden et al. 2004). Increases in CO_2 and water vapour make the above-cloud atmosphere less transparent for LW radiation, thus making OLR less sensitive to the presence of clouds and reducing the LW CRE for unchanged cloud cover. The excessively negative cloud LW contribution also implies that LW_{CLEAR} exaggerates the clear-sky LW contribution to the simulated warming.

The annual multimodel mean warming is on the average 0.89 K larger over land (2.46 K) than sea (1.57 K). The largest contributor to this difference is *SURF*, which has little impact over land but cools the oceans by 0.53 K. LW_{CLEAR}, SW_{CLOUD} and SW_{ALBEDO} also increase the land-sea contrast (by 0.28, 0.25 and 0.12 K, respectively). On the other hand, *CONV* moderates this contrast by 0.40 K, cooling land but warming the oceans. Anomalous heat transport from land to ocean develops during transient increase of atmospheric CO_2, thus spreading the effect of the ocean heat uptake from the oceans to the continents (Lambert et al. 2011).

The terms LW_{CLEAR}, $SW_{CLEAR\text{-}ATM}$ and SW_{ALBEDO} are nearly uniformly positive. Therefore, their multimodel global annual means also give a good idea of their typical local and monthly absolute values even for individual models (right half of Table 2). By contrast, LW_{CRE}, SW_{CLOUD}, *SURF* and *CONV* vary commonly in sign. They thus have much larger values in individual models, months and grid boxes than the multimodel global annual means would suggest. In particular, the mean absolute values of both *SURF* and *CONV* over ocean exceed 2 K.

To the extent that LW_{CRE} and SW_{CLOUD} are dominated by changes in cloud amount, a partial cancellation between them would be expected. Consistent with this, the sum of LW_{CRE} and SW_{CLOUD} (*CLOUD*) has in all columns of Table 2 a smaller magnitude than one or both of these terms individually. In the rest of this paper, we will therefore focus on *CLOUD* rather than its two parts. *SURF* and *CONV* also tend to oppose each other, particularly over the oceans, where *SURF* is much larger than over land. Combining (1), (4) and (6) gives

$$\Delta(S-L) = \Delta G - \Delta\left(C - \frac{\partial E}{\partial t}\right) = -D(SURF + CONV) \qquad (9)$$

The compensation between *SURF* and *CONV* thus implies $\left|\Delta(S-L)\right| < \left|\Delta G\right|$ which means that the net TOA radiation balance changes typically less than the net surface energy flux.

4.2 Annual mean temperature change

The decomposition of the annual mean temperature change to its main components is depicted on maps in Fig. 1. Along with the multimodel mean (first column), two measures are used to characterize the intermodel relationship between the components and the total change ΔT: correlation (second column) and the contribution to standard deviation (right column). The latter is defined as

$$SDC_i = \frac{\overline{\Delta T_i{}'\Delta T{}'}}{\sqrt{\overline{(\Delta T{}')^2}}} = r_i\sqrt{\overline{(\Delta T_i{}')^2}} \qquad (10)$$

where the overbars indicate multimodel averages and the primes deviations from them. The last expression shows that SDC_i is affected by both the correlation of the component *i* with the total temperature change (r_i) and the intermodel standard deviation of this component. The SDC_i:s are additive and sum up to the standard deviation of ΔT.

LW_{CLEAR} widely dominates the multimodel mean warming (Fig. 1d). Its intermodel variations tend to be strongly correlated with ΔT (Fig. 1e), and the highest correlations (> 0.9) mostly occur in those mid-to-high-latitude areas where the intermodel differences in ΔT are large (Fig. 1c). These positive correlations reflect, presumably to a large extent, the water vapour feedback that enhances the greenhouse effect most strongly in the models with the largest warming. Still, the SDC of LW_{CLEAR} (Fig. 1f) falls clearly short of the standard deviation of ΔT (Fig. 1c), particularly at extratropical latitudes. Thus, LW_{CLEAR} substantially amplifies intermodel differences in temperature change but may not generally be the ultimate driver of these differences. The spatial distribution of the multimodel mean warming is also not properly explained by LW_{CLEAR} alone.

$\boldsymbol{SW_{CLEAR\text{-}ATM}}$ is small in the multimodel mean (Fig. 1g) and makes a minute contribution to intermodel variations in temperature change (Fig. 1i). However, it correlates positively with ΔT particularly over the oceans (Fig. 1h), presumably because water vapor increases more in models with larger warming.

$\boldsymbol{SW_{ALBEDO}}$ enhances the multimodel mean warming where snow and ice are reduced. Although modest when globally averaged, its contribution locally exceeds 2 K over (e.g.) the Barents Sea, the Hudson Bay and the Tibetan plateau (Fig. 1j). There is a strong positive intermodel correlation between SW_{ALBEDO} and ΔT over the Arctic and Antarctic oceans and parts of the northern hemisphere extratropical continents (Fig. 1k), where this terms also substantially amplifies the intermodel standard deviation (Fig. 1l).

CLOUD reduces the multimodel mean warming by over 1 K over the Southern Ocean and the northern North Atlantic (Fig. 1m), in both cases mainly due to a negative SW contribution associated with increased cloud cover. The largest positive values over the eastern tropical Pacific and the Arctic Ocean reflect an increase in the LW CRE, and are also connected to increased cloudiness. *CLOUD* is positively correlated with the simulated warming in most parts of the world (Fig. 1n), and its contribution to the intermodel standard deviation of ΔT approaches that of LW_{CLEAR} (Fig. 1o).

SURF plays a large role over the oceans. Although its contribution is negative in most areas, the geographical variation is huge, ranging from a multimodel mean cooling of up to 10 K to the south of Greeland to a warming of 5 K in the Barents Sea (Fig. 1p). *SURF* and ΔT are strongly correlated near the sea ice edge in both hemispheres, as well as in the northwestern North Atlantic (Fig. 1q). In these regions, intermodel differences in temperature change are substantially amplified by changes in the net surface flux, or ultimately by sea ice and ocean circulation changes that regulate the net air-sea heat exchange (Fig. 1r).

Over land, *SURF* is much smaller than over the oceans, with compensating positive and negative values in different months (see Fig. 4 for examples). Yet it does not fully average out in the annual mean. This is mainly due to changes in snowfall (which imply changes in the energy consumed by snow melt) and, primarily over Greenland and Antarctica, increased melting of glacier ice.

As already seen from Table 2, ***CONV*** tends to oppose *SURF* over the oceans (Figs. 1s and 1p). For example, in the northern North Atlantic where the atmosphere loses heat to the surface, this is primarily compensated by increased heat flux convergence and the effect on the local temperature change is thus dampened. Therefore, *CONV* generally reduces the spatial gradients in warming over the oceans (compare Figs. 1s and 1a). In most areas, it also reduces the intermodel differences (Fig. 1u).

CONV slightly reduces the multimodel mean warming in most land areas (Fig. 1s). Exceptions include, among others, Greenland and eastern Antarctica. The Greenland and Antarctic ice sheets also stand out as areas with a substantial positive intermodel correlation between *CONV* and ΔT (Fig. 1t). Thus, unlike in most parts of the world, changes in heat flux convergence act to amplify intermodel differences in temperature change over Greenland and Antarctica (Fig. 1u).

4.3 Seasonality of temperature changes

The effect of the individual energy balance terms on the seasonality of the multimodel mean temperature change is studied in Fig. 2. The seasonality is measured here by the intermonthly standard deviation of ΔT (Fig. 2a). The largest values in the Arctic and over the high-latitude Southern Ocean result from greater warming in late fall and winter than in summer, while the warming in summer slightly exceeds that in winter in many lower-latitude regions (Christensen et al. 2007).

Figures 2c-h show the contributions of the main energy balance components to the intermonthly standard deviation of the temperature change, using the analogy of (10) but with intermodel variations replaced by intermonthly variations. LW_{CLEAR} and *CLOUD* make major contributions to the change in seasonality in large parts of the world. *SURF* is also important in many areas, particularly over the Arctic Ocean and the high-latitude Southern Ocean, where sea ice is reduced. Conversely, SW_{ALBEDO} reduces the seasonality of temperature changes in the Arctic and over the high-latitude Southern Ocean. *CONV* is important in many regions but its contribution varies in sign. Notably, *CONV* strongly damps the seasonality of temperature changes over the Arctic Ocean but amplifies it immediately to the south in northern North America and Eurasia.

To exemplify the factors that regulate the seasonality of temperature change and its intermodel differences, four oceanic and four continental regions are chosen for a closer study. See Fig. 2b for a map of the regions and Table 3 for their boundary coordinates. For each region, the left-hand-side panels in Figs. 3-4 show the contributions of the various energy balance terms to the multimodel mean temperature change, whereas the right-hand-side shows their contributions to the intermodel standard deviation. The latter are first calculated for each grid box separately and then averaged over the domain considered. This order of calculation avoids the systematic effect of the domain size (smaller standard deviations for larger domains) that would occur if calculating the area means before the standard deviations. Both the mean change and the standard deviation contributions vary within the regions, but the main area-averaged results were found to be robust to small changes in the delineation of the areas. Note, however, that the scales in Figs. 3-4 differ from region to region due to the widely varying magnitude of the mean warming and the intermodel differences.

4.3.1 Examples for oceans

The multimodel mean warming over the **Arctic Ocean (AO)** (Fig. 3a) is strongly seasonal, ranging from 1 K in June and July to 9 K in November. This seasonality is driven primarily by *SURF*, which amplifies the warming in autumn and winter but strongly damps it in summer. Reduced ice cover allows the ocean to absorb more SW radiation during the summer, and this heat is released back to the atmosphere in autumn and winter when thinner and less extensive ice cover enhances the heat flux from the relatively warm ocean to the cold atmosphere (Sejas et al. 2014a). LW_{CLEAR} and to some extent *CLOUD* also enhance the seasonality of the warming. SW_{ALBEDO} in isolation would induce a summer maximum of warming, but the resulting heat gain is stored by the ocean. *CONV* also damps the seasonality with a positive contribution in summer (when the Arctic Ocean warms less than the surrounding land areas) and a negative contribution from October to December (when the warming is greatest over the Arctic Ocean). In the annual multimodel area mean, both *SURF* and *CONV* nearly average out.

In most cases, those energy balance terms that increase the multimodel mean warming also tend to increase the intermodel differences over the Arctic Ocean and vice versa (Fig. 3b). The main exceptions are *SURF*, which acts to increase the intermodel differences in all months except from May to July, and *CONV*, which reduces these differences throughout the year but most strongly in autumn and winter.

The ensemble mean warming in the **Northern North Atlantic (NNA)** is small throughout the year, but with a minimum in late spring and a maximum in autumn and winter (Fig. 3c). It mainly represents a balance between large cooling due to *SURF* and warming by *CONV*, but LW_{CLEAR} and *CLOUD* also make non-negligible contributions. Both LW_{CRE} and SW_{CLOUD} are negative, but the latter dominates in spring and summer (not shown). In these seasons, cloud cover increases, presumably due to increased lower-tropospheric stability over a local minimum in the surface warming. Intermodel differences of temperature change in the northern North Atlantic are dominated by differences in *SURF* for most of the year, but in summer *CLOUD* makes the largest contribution (Fig. 3d). Again, *CONV* systematically reduces the intermodel differences.

In the **Tropical East Pacific (TEP)**, the multimodel mean warming is about 40% smaller than the contribution of LW_{CLEAR} alone (Fig. 3e). At the annual mean level, this is mostly due to *CONV*, i.e. increased atmospheric energy transport out of the region. However, although the simulated warming is nearly seasonally invariant, the contributions of the individual energy balance terms vary. During the northern winter and spring, LW_{CLEAR} is mainly moderated by *CONV*, but in summer and autumn, *SURF* overtakes its role. *CLOUD* slightly enhances the multimodel mean warming in most of the year, but is also the main contributor to intermodel differences in temperature change (Fig. 3f). As in the previous regions, *CONV* strongly attenuates the intermodel differences in warming.

The ensemble mean warming over the **Southern Ocean (SO)** is relatively small overall, but has its maximum during the local winter (Fig. 3g). As in the northern North Atlantic, *SURF* attenuates the warming but is counteracted by *CONV*, although both of these are smaller in magnitude. Similar to the northern North Atlantic, *CLOUD* also reduces the warming, particularly in the southern summer when increased cloud cover makes SW_{CLOUD} strongly negative (not shown). *CLOUD* together with LW_{CLEAR} seemingly explains the seasonal cycle of the warming, but the interpretation is complicated because several physically intermingled terms are important in the balance. The same applies to the intermodel differences in warming (Fig. 3h). In particular, although SW_{ALBEDO} acts to amplify these differences in spring and early summer, its influence is moderated by the simultaneous negative contribution from *SURF*. In those models and grid boxes in which the surface albedo decreases due to sea ice melting, the heat gain is stored in the ocean and has limited impact on the local surface temperature. This closely resembles the situation in the Arctic Ocean in the summer.

4.3.2 Examples for land areas

The ensemble mean warming in **Siberia (SIB)** is largest in early winter and smallest in summer (Fig. 4a). This seasonality is largely driven by *CONV*, which enhances the warming in the winter half-year but strongly reduces it from May to

August. The patterns in Fig. 2h suggest that this primarily reflects heat exchange with the Arctic Ocean, where the warming is larger than in Siberia in late autumn and winter but smaller in summer. Due to earlier snow melt, SW_{ALBEDO} substantially contributes to the warming in spring and early summer, but the resulting heat gain is counteracted by increased atmospheric energy divergence out of the area. *SURF* is also negative in April and May but positive in summer. Snowmelt occurs earlier in a warmer climate (e.g., Räisänen 2008), and the associated energy sink is thus enhanced (reduced) early (late) in the melting season.

SW_{ALBEDO} makes a large contribution to intermodel differences in temperature change in Siberia in spring and early summer (Fig. 4b), but this is largely compensated by a negative contribution from *CONV* in the same season. By contrast, *CONV* slightly amplifies the intermodel differences in late autumn and winter. In summer, *CLOUD* also increases the intermodel differences in temperature change.

In **Central Europe (CEU),** *CONV* reduces the ensemble mean warming, keeping it below the contribution of LW_{CLEAR} in most of the year (Fig. 4c). The exception is late summer (July-September), when a positive *CLOUD* contribution due to reduced cloudiness amplifies the simulated warming, thus explaining its annual maximum in this season. More strikingly, *CLOUD* strongly amplifies the intermodel differences in warming in the summer half-year, although being counteracted by *CONV* (Fig. 4d). In winter, *CONV* slightly enhances the intermodel differences in warming.

In a surprising contrast with the seasonal cycle of LW_{CLEAR}, the multimodel mean warming in **Amazonia (AMZ)** is slightly larger in the southern hemisphere winter and spring than in summer and autumn (Fig. 4e). This is largely due to *CONV*, which reduces the warming less in winter than in summer. Intermodel differences in warming in Amazonia are mainly attributed to LW_{CLEAR}, *CONV* and *CLOUD*. They are largest during the southern winter and spring, when the contribution of *CONV* has its maximum.

The warming over **Antarctica (ANT)** is nearly seasonally uniform (Fig. 4g). This results fom a compensation between the seasonalities of *CLOUD*, *SURF*, *CONV* and $SW_{CLEAR\text{-}ATM}$. Interestingly, $SW_{CLEAR\text{-}ATM}$ enhances the warming by up to 0.6°C during the Antarctic summer when solar radiation is abundant. Intermodel differences in temperature change over Antarctica are amplified by *CONV* throughout the year, although most strongly in the autumn and winter (Fig. 4h). Other major contributors to these differences include LW_{CLEAR} and *CLOUD*.

4.4 Discussion

As shown above, different energy balance terms dominate the intermodel spread of temperature change in different seasons and areas. For a simple overview, Fig. 5 identifies the terms that make the largest local contributions to the standard deviation of the annual mean temperature change based on the values shown in the third column of Fig. 1. LW_{CLEAR} and *CLOUD* are the most prominent terms, making the largest contributions in 34% and 29% of the global area. *CLOUD* is important particularly over lower-latitude oceans, but is rarely the largest uncertainty over land. The third most important term in terms of the area of domination is *SURF*, being largest in 20% of the global area and 27% of the oceans. *CONV* dominates the uncertainty in 10% of the world, including parts of the Greenland and Antarctic ice sheets. SW_{ALBEDO} has a share of 8%, ranking as first e.g. in eastern Siberia, Tibet and parts of the Southern Ocean. A broadly similar picture arises if the dominance is counted on a monthly rather than annual basis, although *CONV* tends to grow more important in this case (not shown).

Another aspect deserving discussion is the behaviour and physical interpretation of *CONV*. The first hypothesis that one can make is that *CONV* acts as diffusion-like process, smoothing out the spatial gradients in temperature change (Boer and Yu 2003). This could happen under unchanged atmospheric circulation as eddies spread out regional differences in temperature change, but the circulation might also adjust to transport more energy from areas of larger warming to areas of smaller warming. Alternatively, circulation changes not directly related to the distribution of the near-surface warming could play a more active role in shaping the temperature response.

While not precluding the second alternative, our results give much more evidence for the first. First, Figs. 1a and 1s reveal that *CONV* frequently moderates the local extremes and gradients of ΔT. Examples of this include the maximum in warming over the Barents Sea and the minima over the northern North Atlantic and the Southern Ocean, as well as the land-sea contrast of warming across several coastlines. As expected for a diffusion-like process, this tendency for compensation is stronger at small than large spatial scales. The global spatial correlation between ΔT and *CONV* is only slightly negative (-0.22). However, it becomes more negative (-0.43) when large-scale features are filtered out from both fields by using a radius of 2000 km in the smoothing algorithm of Räisänen and Ylhäisi (2011) and retaining the small-scale component.

Second, also consistent with the diffusion hypothesis, *CONV* more commonly reduces than amplifies the intermodel differences of temperature change (Figs. 1t-u). It is the only term in our decomposition that does this in a globally averaged sense. However, this tendency is not globally uniform. The correlation between *CONV* and ΔT is less regularly negative over land than oceans, and some land areas (most notably Greenland and Antarctica) stand out with a substantial positive correlation (Fig. 1t).

There are two probable reasons for the stronger anticorrelation between *CONV* and ΔT over the oceans. First, the homogeneity of the ocean surface suggests a tighter coupling between the surface and free tropospheric temperature changes than is the case over more heterogeneous land areas. Large local gradients in the surface air temperature change over the oceans would thus imply large gradients in the change of tropospheric temperatures, which would be dynamically unsustainable (Joshi et al. 2008). Second and perhaps more importantly, the sum of the other temperature change components ($\Delta T_{REST} = \Delta T - CONV$) is much more variable over ocean than land areas (Fig. 6a), essentially due to the larger surface heat flux changes. Thus, there is a larger need for CONV to damp this variability over the oceans.

A very strong anticorrelation prevails between *CONV* and ΔT_{REST} over most of the oceans and also over some land areas (e.g. the Tibetan Plateau) where the intermodel standard deviation of ΔT_{REST} is large (Fig. 6b). Conversely, areas with a local minimum in the intermodel variation of ΔT_{REST} are commonly associated with a weak or even positive correlation between *CONV* and ΔT_{REST}. Examples include the Sahara – Arabian desert, Australia, and most notably Greenland and Antarctica. For both Greenland and Antarctica, a striking contrast between modest local intermodel variations in ΔT_{REST} and much larger variations over the surrounding oceans suggests a remote control of *CONV*. A closer analysis reveals a negative intermodel correlation of *CONV* between the Antarctic continent and the Southern Ocean south of 60°S, and between Greenland and the northern North Atlantic, particularly the Labrador Sea (not shown). This suggests that the local warming over Antartica and Greenland is substantially modulated by heat transport from the surrounding oceans.

5. Conclusions

An energy balance decomposition was conducted for regional temperature changes resulting from a gradual doubling of atmospheric CO_2 concentration in 16 CMIP5 models. A simple method was applied that links the surface air temperature with the OLR by using an effective emissivity as a measure of the atmospheric greenhouse effect. The method is rough in its treatment of LW radiation, and can therefore not separate the effects of the direct CO_2 forcing and the water vapour and lapse rate feedbacks from each other. SW radiative processes are treated in more detail using the APRP method (Taylor et al. 2007). Additionally, temperature changes due to the net surface flux and atmospheric energy flux convergence changes are calculated. The method only requires two-dimensional model output for the surface and the TOA, and is therefore easy to apply to large ensembles of climate model simulations.

As expected, the bulk of the simulated warming was found to be due to an enhanced clear-sky greenhouse effect. However, other components of the energy balance substantially modify the temperature change, particularly its geographical, seasonal and intermodel variations.

In particular, we found that changes in horizontal atmospheric energy flux convergence mostly act as a diffusion-like process, thus reducing horizontal gradients and intermodel differences in temperature change. This is the case especially over the oceans, but energy convergence changes also typically moderate the intermodel differences over those land areas where the net effect of the other terms would result in a large intermodel variation of warming. However, Greenland and Antarctica are important counter-examples. Intermodel variability in the other energy balance terms is relatively modest over both Greenland and Antarctica, but changes in the net surface energy flux and surface albedo make it much larger over the surrounding sea areas. Changes in energy flux converge act to spread the effects of this larger variability over Greenland and Antarctica, thus amplifying intermodel differences in temperature change over these ice sheets.

Changes in the net surface heat flux reduce the multimodel global mean warming by 0.4 K, in close agreement with the value found by DB08 for the CMIP3 models. Regionally, however, this contribution varies from a cooling of up to 10 K over the northern North Atlantic to a warming of 5 K over the Barents Sea. As found earlier by Sejas et al. (2014a) by using the CFRAM method, changes in the net surface energy flux are also crucially important for the seasonal cycle of the warming over the Arctic Ocean.

Several studies have identified cloud feedbacks as the largest uncertainty in global mean temperature change (Flato et al. 2013, Vial et al. 2013). Our analysis extends this finding by indicating that clouds commonly make the largest contribution to intermodel spread of regional temperature change over lower-latitude oceans. However, changes in the clear-sky greenhouse effect (mainly over land) and the net surface energy flux (mainly over extratropical oceans) also dominate the intermodel spread in wide areas.

Our energy balance approach provides an alternative to the CFRAM method (Lu and Cai 2009) and the surface energy budget method of IBH15. All these methods give different perspectives on the energetic causes of regional temperature change, but a direct comparison is difficult because of differences in the set of processes that are explicitly included. The main advantages of the present method are (i) its relative simplicity and modest data needs, which are comparable with the IBH15 approach, and (ii) a partial although not perfect comparability with TOA radiation balance based studies of global mean temperature change, such as DB08. The most obvious weakness is the crude treatment of LW processes. This could be improved by an explicit modelling of LW radiative transfer, but at the cost of increasing the data needs and the complexity of the method.

Acknowledgments

We acknowledge the World Climate Research Programme's Working Group on Coupled Modelling, which is responsible for CMIP, and we thank the climate modeling groups for producing and making available their model output. For CMIP the U.S. Department of Energy's Program for Climate Model Diagnosis and Intercomparison provides coordinating support and led development of software infrastructure in partnership with the Global Organization for Earth System Science Portals. This work was supported by the Academy of Finland Centre of Excellence in Atmospheric Science – From Molecular and Biological processes to the Global Climate (project 272041). The two anonymous reviewers are acknowledged for their constructive comments.

References

Boer GJ, Yu B (2003) Climate sensitivity and response. Clim Dyn 20: 415-429

Boucher O, Randall D, Artaxo P, Bretherton C, Feingold G, Forster P, Kerminen V-M, Kondo Y, Liao H, Lohmann U, Rasch P, Satheesh SK, Sherwood S, Stevens B, Zhang XY (2013) Clouds and Aerosols. In: Stocker TF et al (eds) Climate Change 2013: the Physical Science Basis. Cambridge University Press, pp 571-657

Caldwell PM, Zelinka MD, Taylor KE, Marvel K (2016) Quantifying the sources of intermodel spread in equilibrium climate sensitivity. Journal of Climate 29: 513-524

Christensen JH, Hewitson B, Busuioc A, Chen A, Gao X, Held I, Jones R, Kolli RK, Kwon W-T, Laprise R, Magaña Rueda V, Mearns L, Menéndez CG, Räisänen J, Rinke A, Sarr A, Whetton P (2007) Regional Climate Projections. In Solomon S et al (eds) Climate Change 2007: the Physical Science Basis. Cambridge University Press, pp 847-940

Cubasch U, Meehl GA, Boer GJ, Stouffer RJ, Dix M, Noda A, Senior CA, Raper, SCB, Yap KS (2001) Projections of Future Climate Change. In: Houghton

JT et al. (eds) Climate Change 2001: the Scientific Basis. Cambridge University press, pp 526-582

Dufresne J-L, Bony S (2008) An assessment of the primary sources of spread of global warming estimates from coupled atmosphere-ocean models. J Climate 21: 5135-5144

Flato G, Marotzke J, Abiodun B, Braconnot P, Chou SC, Collins W, Cox P, Driouech F, Emori S, Eyring V, Forest C, Gleckler P, Guilyardi E, Jakob C, Kattsov V, Reason C, Rummukainen M (2013) Evaluation of Climate Models. In: Stocker TF et al (eds) Climate Change 2013: the Physical Science Basis. Cambridge University Press, pp 741-866

Gregory JM, Mitchell JFB (1997) The climate response to CO_2 of the Hadley Centre coupled AOGCM with and without flux adjustment. Geophys Res Lett 24: 1943-1946

Hansen J, Lacis A, Rind D, Russell G, Stone P, Fung I, Ruedy R, Lerner J (1984) Climate sensitivity: Analysis of feedback mechanisms. In: Hansen JE, Takahashi T (eds) Climate Processes and Climate Sensitivity. Geophysical Monograph 29, Maurice Ewing Vol. 5, American Geophysical Union, pp. 130-163

Houghton J (2015) Global Warming. The Complete Briefing, 5th edition. Cambridge University Press, 380 pp

Izumi K, Bartlein PJ, Harrison SP (2015) Energy-balance mechanisms underlying consistent large-scale temperature responses in warm and cold climates. Clim Dyn 44: 3111-3127

Joshi MM, Gregory JM, Webb MJ, Sexton DMH, Johns TC (2008) Mechanisms for the land/sea warming contrast exhibited by simulations of climate change. Clim Dyn 30: 455-465

Lambert HF, MJ Webb, Joshi MM (2011) The relationship between land-ocean surface temperature contrasts and radiative forcing. J Climate 24: 3239-3256

Lu J, Cai M (2009) A new framework for isolating individual feedback processes in coupled general circulation climate models. Part I: formulation. Clim Dyn 32: 873-885

Qu X, Hall A (2006) Assessing snow albedo feedback in simulated climate change. J Climate 19: 2617-2630

Räisänen J (2008) Warmer climate: less or more snow? Clim Dyn 30: 307-319

Räisänen J, Ylhäisi JS (2011) How much should climate model output be smoothed in space? J Climate 24: 867–880

Räisänen J, Ylhäisi JS (2015) CO_2-induced climate change in northern Europe: CMIP2 versus CMIP3 versus CMIP5. Clim Dyn 45: 1877–1897

Sejas SA, Cai M, Hu A, Meehl GA, Washington W, Taylor PC (2014a) Individual feedback contributions to the seasonality of surface warming. J Climate 27: 5653-5659

Sejas SA, Albert OS, Cai M, Deng Yi (2014b) Feedback attribution of the land-sea warming contrast in a global warming simulation of the NCAR CCSM4. Environ Res Lett 9: 124005

Soden BJ, Held IM (2006) An assessment of climate feedbacks in coupled ocean atmosphere models. J Climate 19: 3354-3360

Soden BJ, Broccoli AJ, Hemler AS (2004) On the use of cloud forcing to estimate cloud feedbacj. J Climate 17: 3661-3665

Taylor KE, Crucifix M, Braconnot P, Hewitt CD, Doutriaux C, Broccoli AJ, Mitchell JFB, Webb MJ (2007) Estimating shortwave radiative forcing and response in climate models. J Climate 20: 2530-2543

Taylor PC, Cai M, Hu A, Meehl GA, Washington W, Zhang GJ (2013) A decomposition of feedback contributions to polar warming amplification. J Climate 26: 7023-7043

Tomassini L, Geoffroy O, Dufresne J-L, Idelkari A, Cagnazzo C, Block K, Mauritsen T, Giorgetta M, Quaas J (2013) The respective roles of surface temperature driven feedbacks and tropospheric adjustment to CO_2 in CMIP5 transient climate simulations. Clim Dyn 41: 3103-3126

Vial J, Dufresne J-L, Bony S (2013) On the interpretation of inter-model spread in CMIP5 climate sensitivity estimates. Clim Dyn 41: 3339-3362

Zhao W, Kuhn WR, Drayson SR (1994) The significance of detailed structure in the boundary layer to thermal radiation at the surface in climate models. Geophys Res Lett 21: 1631-1634

Tables

***Table 1**. List of the variables used*

CMIP5 Acronym	Long name
tas	near-surface air (2-meter) temperature
rsdt	TOA incident SW radiation
rsut	TOA outgoing SW radiation
rlut	TOA outgoing LW radiation
rsds	surface downwelling SW radiation
rsus	surface upwelling SW radiation
rlds	surface downwelling LW radiation
rlus	surface upwelling LW radiation
hfls	surface upward latent heat flux
hfss	surface upward sensible heat flux
rsutcs	TOA outgoing clear-sky SW radiation
rlutcs	TOA outgoing clear-sky LW radiation
rsdscs	surface downwelling clear-sky SW radiation
rsuscs	surface upwelling clear-sky SW radiation
clt	total cloud fraction

TOA = top of the atmosphere; SW = shortwave; LW = longwave

Table 2. *Mean values (columns 1-3) and mean absolute values (columns 4-6) of the terms in Eqs. (6)-(8) (unit: K)*

	Global annual multimodel mean			Absolute value of local monthly means in individual models		
	All	Land	Sea	All	Land	Sea
ΔT	1.82	2.46	1.57	1.83	2.46	1.57
LW_{CLEAR}	2.07	2.27	1.99	2.07	2.27	1.99
LW_{CRE}	-0.39	-0.36	-0.41	0.69	0.64	0.72
SW_{IN}	-2×10^{-4}	-2×10^{-4}	-2×10^{-4}	7×10^{-4}	9×10^{-4}	7×10^{-4}
$SW_{CLEAR-ATM}$	0.21	0.26	0.19	0.22	0.27	0.21
SW_{ALBEDO}	0.19	0.28	0.16	0.22	0.34	0.17
SW_{CLOUD}	0.13	0.31	0.06	0.88	0.79	0.92
SW_{NL}	-2×10^{-4}	-4×10^{-5}	-3×10^{-4}	6×10^{-4}	5×10^{-4}	7×10^{-4}
SURF	-0.39	-0.03	-0.53	1.62	0.38	2.12
CONV	0.01	-0.28	0.12	1.74	0.97	2.05
ERR	-3×10^{-4}	-3×10^{-4}	-4×10^{-4}	8×10^{-4}	8×10^{-4}	9×10^{-4}
*CLOUD**	-0.26	-0.04	-0.35	0.75	0.60	0.81
SURF + CONV	-0.38	-0.30	-0.41	0.90	0.88	0.90

*CLOUD = LW_{CRE} + SW_{CLOUD}

Table 3. *The areas used in Figs. 3-4*

Area (acronym in Fig. 2b)	Definition
Arctic Ocean (AO)	Sea (75°-90°N)
Northern North Atlantic (NNA)	Sea (50°-60°N, 10°-50°W)
Tropical East Pacific (TEP)	Sea (5°S-5°N, 80°-180°W)
Southern Ocean (SO)	Sea (50°-65°S)
Siberia (SIB)	Land (50°-75°N, 80°-180°E)
Central Europe (CEU)	Land (45°-55°N, 0°-30°E)
Amazonia (AMZ)	Land (20°S-5°N, 80°-40°W)
Antarctica (ANT)	Land (65°-90°S)

Figures

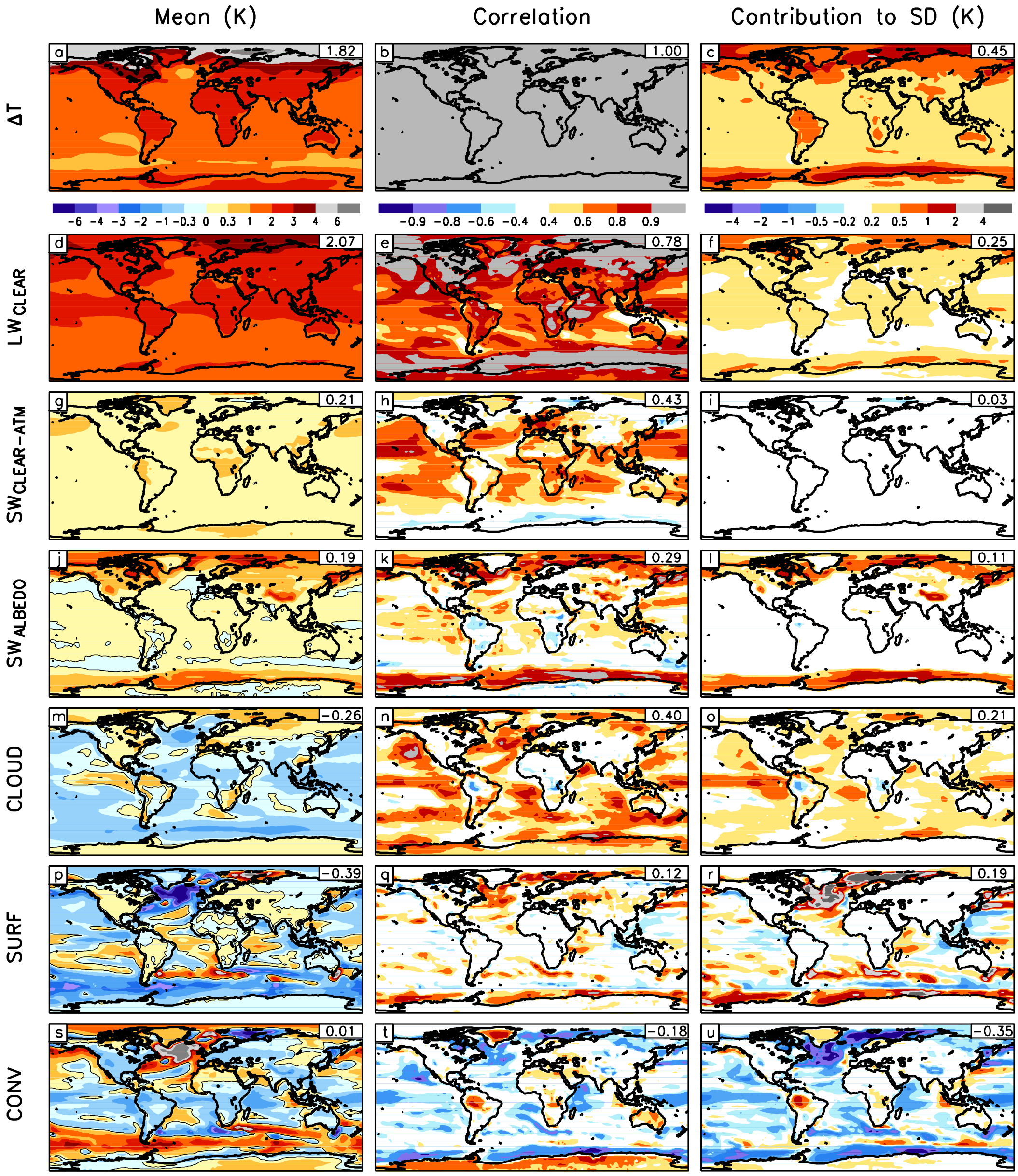

***Fig. 1** Simulated annual mean temperature change ΔT (row 1) and its decomposition (rows 2-7). Left: multimodel means. Middle: intermodel correlation between the individual components and ΔT. Right: the standard deviation of ΔT and the contributions of the individual components to it. The global area means are given in the top-right corner of the panels*

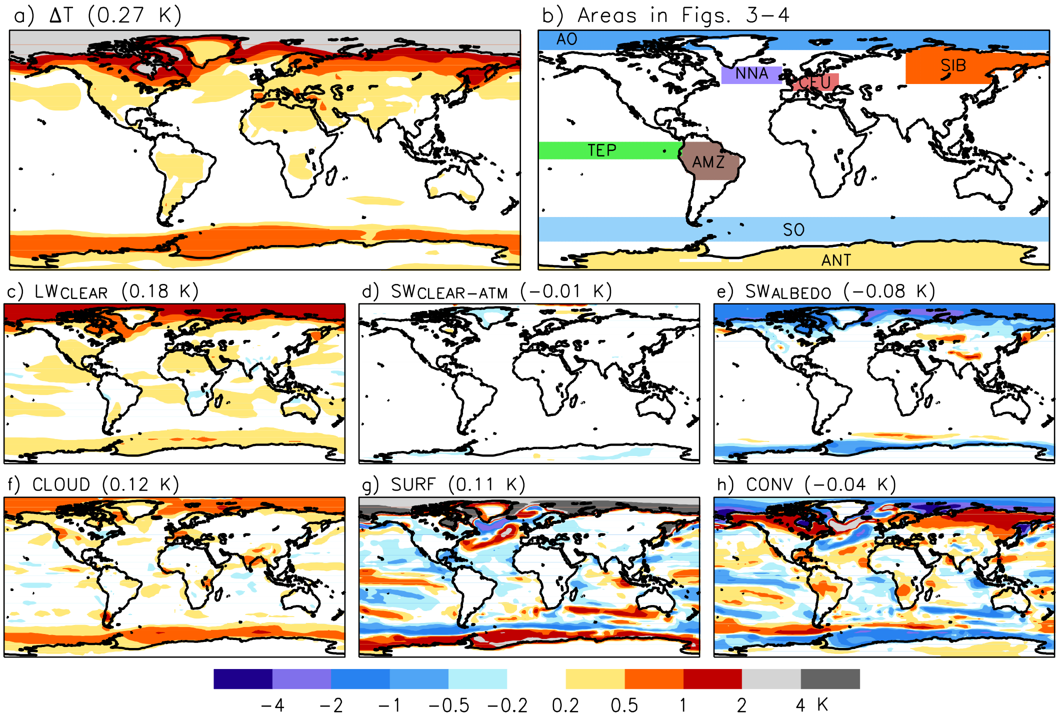

Fig. 2 *Intermonthly standard deviation of the multimodel mean temperature change (a) and the contributions of the six main temperature change components to it (c-h). Panel (b) shows the areas studied in Figs. 3-4, using the acronyms listed in Table 3*

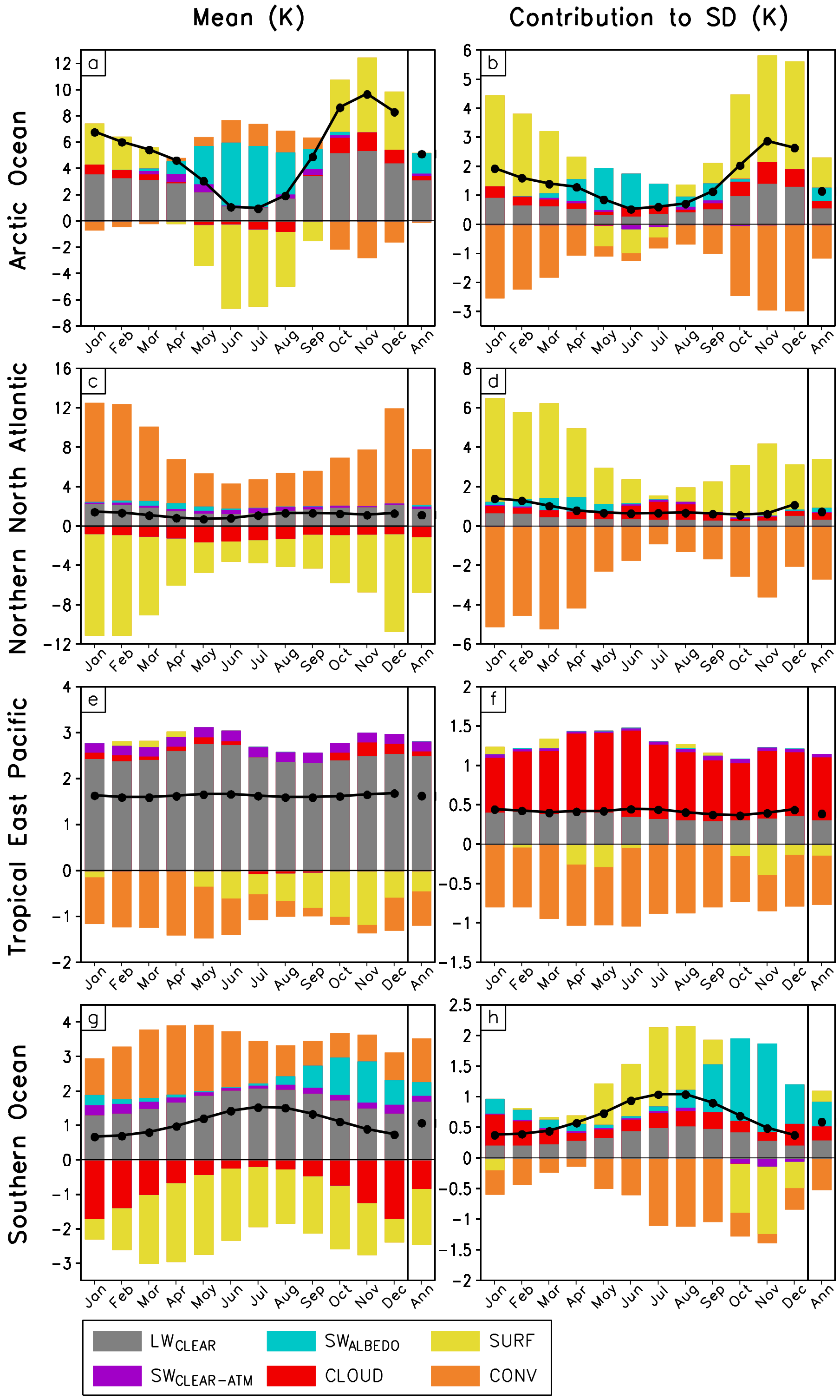

Fig. 3. *Left: contributions of the six main temperature change components to multimodel mean monthly temperature changes in four oceanic regions (see the legend at the bottom; the total change is shown by the solid line). The last bar gives the annual mean values. Right: the corresponding contributions to intermodel standard deviation of temperature change, first evaluated at the grid box scale and then spatially averaged. See Fig. 2b and Table 3 for the definition of the areas*

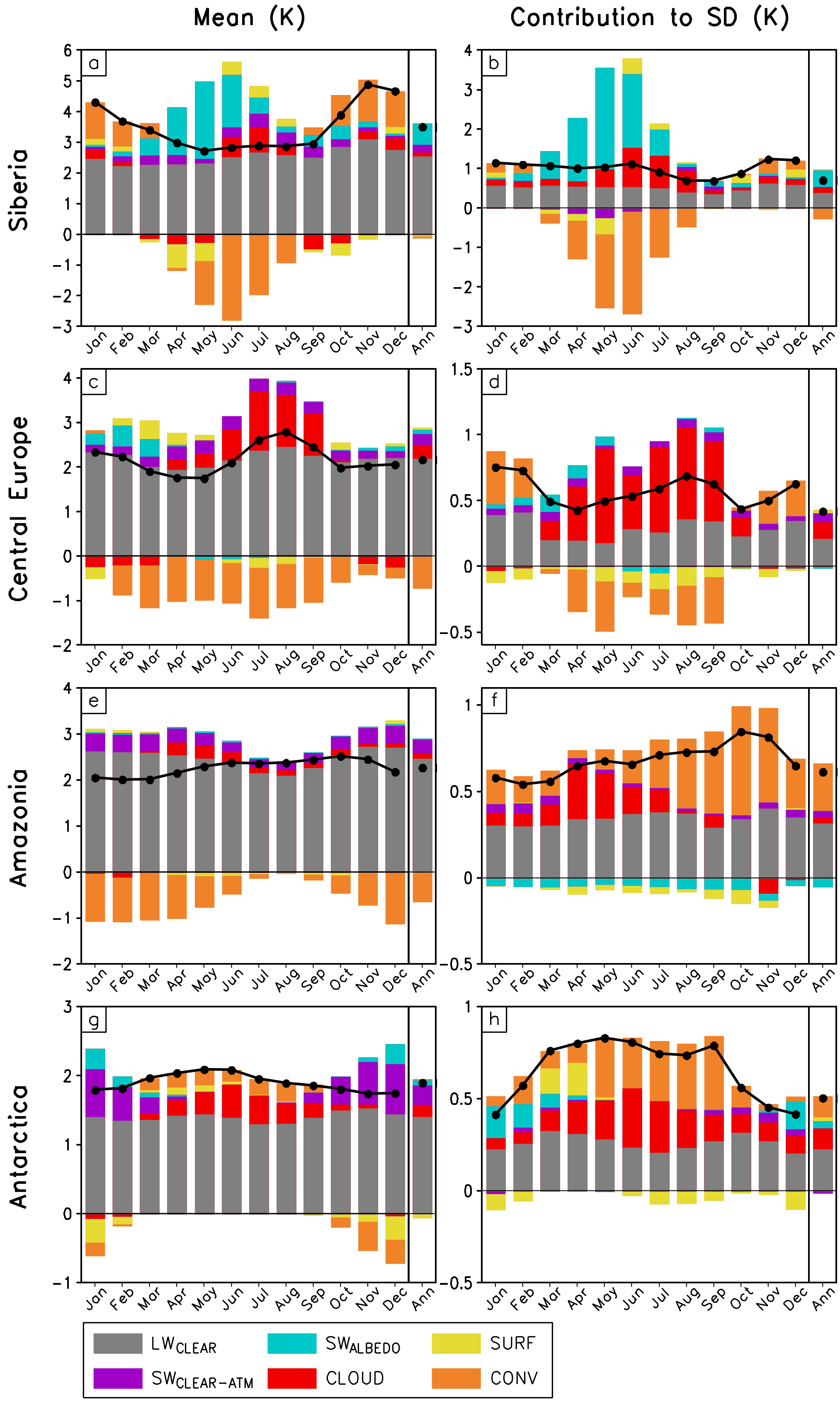

Fig. 4. *As Fig. 3 but for four land areas*

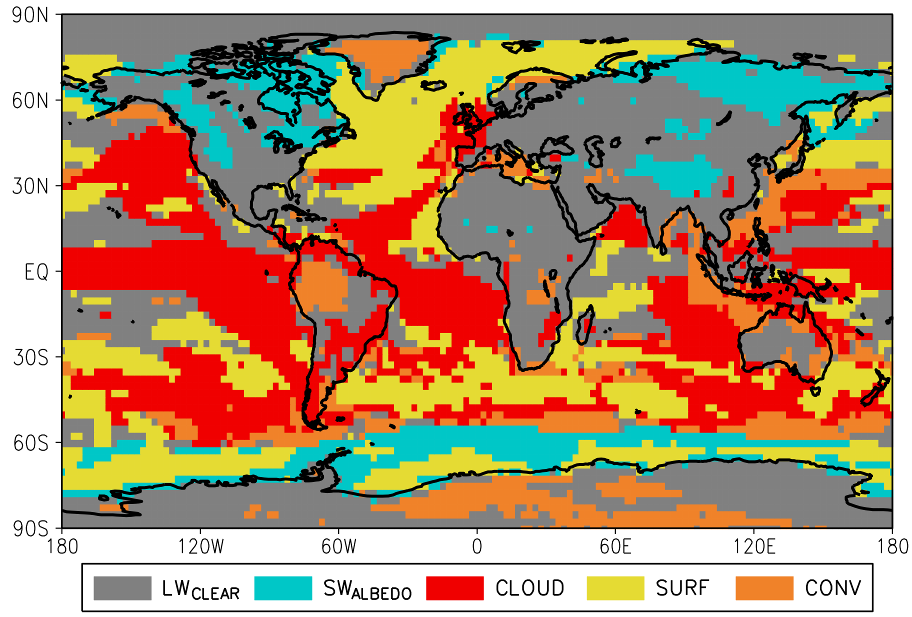

Fig. 5. *The largest energy balance contributors to the standard deviation of annual mean temperature change*

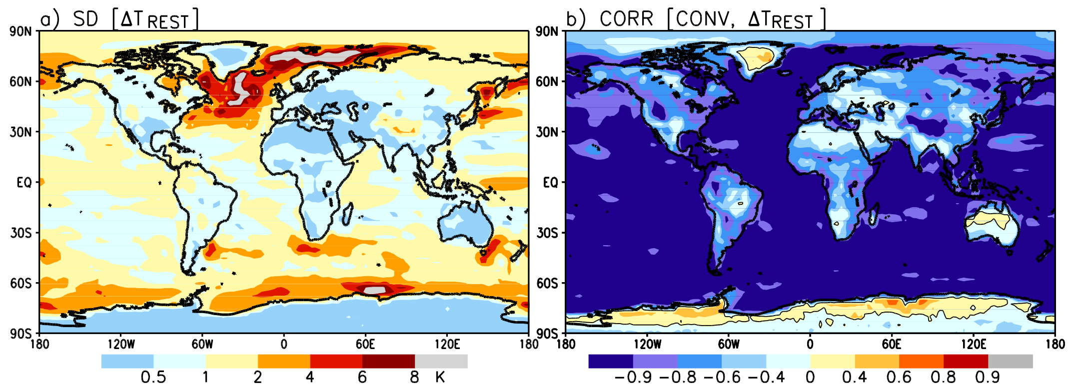

Fig. 6. *(a) Intermodel standard deviation of annual mean ΔT_{REST}. (b) Intermodel correlation between CONV and ΔT_{REST}.*